Korean J. Chem. Eng., 36(1), 84-91 (2019)
DOI: 10.1007/s11814-018-0147-0

pISSN: 0256-1115
eISSN: 1975-7220

Sensitivity analysis of key factors in controlling absorption and desorption of oxygen to oxygen carriers

Limin Hou, Qingbo Yu†, Kun Wang, Shuo Zhang, Qin Qin, and Fan Yang

School of Metallurgy, Northeastern University, No 11, Lane 3, Wenhua Road, Heping District, Shenyang 110819, Liaoning, P. R. China
(*Received 31 May 2018 • accepted 28 August 2018*)

Abstract−Chemical looping air separation gives an oxygen resource for the oxy-fuel combustion system. To investigate the sensitivity of operation parameters and optimal operation parameters, with the consideration of the reactor temperature, we used the oxygen concentration, and reaction gas flow, an orthogonal experiment and multi-objective comprehensive evaluation method to analyze the results obtained by fixed-bed apparatus with the $YBaCo_4O_{7+\delta}$, $Y_{0.95}Ti_{0.05}BaCo_4O_{7+\delta}$, $Y_{0.5}Dy_{0.5}BaCo_4O_{7+\delta}$ and $Y_{0.2}Ti_{0.05}Dy_{0.75}BaCo_4O_{7+\delta}$ oxygen carriers. The results showed that the effects of operating conditions on oxygen absorption/desorption properties varieds in the order: oxygen concentration>gas flow rate>absorption temperature=desorption temperature. Analysis of max-min difference showed that the optimum operating conditions such as absorption temperature, 350 °C, desorption temperature, 430 °C, gas flow rate, 200 ml/min, and oxygen concentration, 21% were confirmed.

Keywords: Orthogonal Test, Multi-objective Comprehensive Evaluation, Oxygen Carrier, Sensitivity, Optimum Analysis

INTRODUCTION

With the increasing trend of fossil fuel combustion, huge amount of CO_2 is emitted to the atmosphere, which is the dominating contributor to global warming. An efficient and economic technology for CO_2 separation is urgently needed. Oxyfuel combustion, considered as one of the most potential technologies to reduce the CO_2 emission, was conducted in the process of O_2/CO_2 recycle combustion, in which 95% or higher oxygen concentration is needed [1]. O_2 plays an essential role in the oxyfuel combustion system. However, oxyfuel combustion technology has not been applied in industry widely as the high cost of oxygen production. Chemical looping air separation (CLAS), with the characteristics of cost-effective, energy-extensive and operation-simplicity in the oxygen production process, proposed by Moghtaderi in 2010, is a non-traditional air separation technology [2]. The CLAS process can save 74% of the power of the cryogenic air separation process [2]. A schematic of the CLAS process is described elsewhere [2,3]. Oxygen carrier is the essential core of the CLAS system. The metal oxide oxygen carriers such as Cu-based, Co-based, and Mn-based have caught the attention of researchers [4-17]. Song et al. investigated the kinetics of CuO/SiO_2 oxygen carriers in a CLAS system using the TGA data [4]. The results indicated that the phase boundary reaction model (R2) and random nucleation and subsequence growth model (A2) were fitted well with oxidation and reduction process, respectively. Chuang et al. investigated the oxidation/reduction properties of CuO/Al_2O_3 oxygen carriers in a fluidized bed [5]. The results indicated that oxygen carriers showed good performance of activity and stability within 18 cycles. Wang et al. investigated the reduction kinetics of CuO/TiO_2, CuO/ZrO_2, and CuO/SiO_2 oxygen carriers in a CLAS system using the TGA data [6]. The results indicated that random nucleation and subsequence growth model were fitted well with the reduction process. Mattisson et al. investigated the thermodynamic properties of Mn_3O_4, CuO, and CoO oxygen carriers in a CLC (chemical looping combustion) system by the thermodynamic simulations [9]. The results of thermal analysis indicated that Mn_2O_3/Mn_3O_4 and CuO/Cu_2O were the most promising. And, tests on CuO with gaseous and solid fuel indicated that CLC process can be possible.

Metallic oxide oxygen carriers react at high temperature, consuming large amount of energy. Researchers showed that flue gas can be utilized as a high temperature heat resource of metallic oxide oxygen carriers [18,19]. However, although the waste heat of high temperature has been used effectively in industry, the waste heat of low temperature has not. If oxygen carriers can work at low temperature, the problem of high energy-consumption can be resolved. $YBaCo_4O_{7+\delta}$, donating Y114 phase, is highly potential candidate for oxygen carriers working at low temperature. The compound was originally synthesized by Valldor and Andersson [20]. Karppinen et al. found that $YBaCo_4O_{7+\delta}$ showed two processes of oxygen absorption and desorption, if heated from ambient temperature to 1,100 °C in oxygen containing atmosphere [21]. The first process occurred at about 200 °C-400 °C. The maximum oxygen content achieved was $\delta \approx 1.0$ and $\delta \approx 1.2$ in air and oxygen atmosphere, respectively. The oxygen intake/release process, controlled by oxygen partial pressure or/and reaction temperature, was highly reversible [22]. $YBaCo_4O_{7+\delta}$, with fine oxygen compatibility, may be suitable for oxygen carrier candidate working at low temperature in CLAS

†To whom correspondence should be addressed.
E-mail: yuqb@smm.neu.edu.cn
Mailing address: P. O., Box345, Northeastern University, No 11, Lane 3, Wenhua Road, Heping District, Shenyang, Liaoning, P. R. China

system. Oxygen content, ($\delta \approx 1.2$, corresponding to the oxygen storage capacity of 1,225 μmol O_2/g) is larger than the theoretical value (870 μmol O_2/g) of conventional oxygen storage materials, CeO_2-ZrO_2 [23,24]. Now, to improve the oxygen storage capacity (OSC), researches on the substitution in Y site with Ca, Zr, Dy, Tb, Ho, Er, Lu, Yb, and Tm [21,25-31] have been developed. The results showed that Zr, Dy, and Tb substitution had positive effects on enhancing the OSC.

The researches about the effects of operation parameters on the oxygen intake/release properties of 114 phase oxygen carriers are very scant. Operation parameters such as absorption temperature/time, desorption temperature/time, gas flow rate, oxygen concentration, and particle size play a vital role in intaking/releasing properties of 114 phase oxygen carriers, which is rarely reported in the literature. It is necessary to investigate the sensitivity of operation parameters for the rate of oxygen absorption/desorption and amount of oxygen absorption/desorption, which is significant for the oxygen intaking/releasing behaviors of 114 phase oxygen carriers. What's more, the optimal operation parameters are also significant for the oxygen intaking/releasing behavior of oxygen carriers. In this study, the sensitivity and optimal operation parameters were investigated by orthogonal experiment combined with multi-objective comprehensive evaluation method with monolithic oxygen carriers in a fixed-bed reactor. The obtained results help identify the influence level of operation parameters and optimal operation parameters for practical design of a separation process based on 114 phase oxygen carriers for oxygen production in the future.

EXPERIMENTAL SECTION

1. Preparation of Materials

Samples $YBaCo_4O_{7+\delta}$, $Y_{0.95}Ti_{0.05}BaCo_4O_{7+\delta}$, $Y_{0.5}Dy_{0.5}BaCo_4O_{7+\delta}$, $Y_{0.2}Ti_{0.05}Dy_{0.75}BaCo_4O_{7+\delta}$ were synthesized by solid-state reaction [27]. Cordierite honeycombs with cell density of 400 CPSI and wall thickness 0.15 mm were used. The cordierite honeycombs were calcined at 900 °C before being used [33]. The slurry was prepared by mixing appropriate stoichiometric amount of the active phase, Al_2O_3 sol and deionized water with ultrasonic vibration [34], followed by adjusting the pH of solution to 3.5 [35]. The excess slurry was removed by blowing air through the channels. Cordierite honeycombs were washcoated by oxygen carrier by dipping samples in the slurry with the slurry washcoating method [34]. In this case, the monolith sample was suspended in continually vibrating solution [36]. Several times of impregnation were needed until the desired amount of loading was obtained, about 30 wt% of the cordierite honeycomb [33]. After cycles, the monolithic samples were dried at room temperature and dried overnight at 100 °C, followed by calcining at 550 °C for 3 h to stabilize γ-Al_2O_3 powder.

2. Experimental Setup

To study the sensitivity of operating conditions and optimal operation parameters, parameters, i.e., for oxygen absorption process, flow rates of the feed gases (200 ml/min, 300 ml/min, 400 ml/min, 500 ml/min), oxygen concentration (5.5%, 10.5%, 15.5%, 21%), adsorption temperature (290 °C, 310 °C, 330 °C, 350 °C), for oxygen absorption process, desorption temperature (390 °C, 410 °C, 430 °C, 450 °C), were investigated with $YBaCo_4O_{7+\delta}$, $Y_{0.95}Ti_{0.05}BaCo_4O_{7+\delta}$, $Y_{0.5}Dy_{0.5}BaCo_4O_{7+\delta}$, $Y_{0.2}Ti_{0.05}Dy_{0.75}BaCo_4O_{7+\delta}$ oxygen carriers. An orthogonal table with five factors and four levels was used to design the experiment scheme, see Table 1. In an orthogonal test, the operating conditions are signed as the experimental factors. Fig. 1 shows a schematic view of the experimental fix-bed system, including a gas delivery system, mass flow rate meter, reactor, a cooling system, online gas analyzer and data acquisition system. The monolithic samples with oxygen carrier mass of 10 g, supported by distributor plate [37], were placed in the fixed-bed reactor (30 mm i.d. and 1,200 mm height). During the absorption process, the monolithic

Table 1. Orthogonal arrays $L_{16}(4^5)$ of experiment scheme

Factor	A	B	C	D	E
Experiment scheme	Oxygen carrier	Absorption temperature/°C	Desorption temperature/°C	Gas flow/ml/min	Oxygen concentration/%
1	1($YBaCo_4O_{7+\delta}$)	1(290)	1(390)	1(200)	1(5.5)
2	1	2(310)	4(450)	3(400)	2(10.5)
3	1	3(330)	2(410)	4(500)	3(15.5)
4	1	4(350)	3(430)	2(300)	4(21)
5	2($Y_{0.95}Ti_{0.05}BaCo_4O_{7+\delta}$)	1	2	2	2
6	2	2	3	4	1
7	2	3	1	3	4
8	2	4	4	1	3
9	3($Y_{0.5}Dy_{0.5}BaCo_4O_{7+\delta}$)	1	3	3	3
10	3	2	2	1	4
11	3	3	4	2	1
12	3	4	1	4	2
13	4($Y_{0.2}Ti_{0.05}Dy_{0.75}BaCo_4O_{7+\delta}$)	1	4	4	4
14	4	2	1	2	3
15	4	3	3	1	2
16	4	4	2	3	1

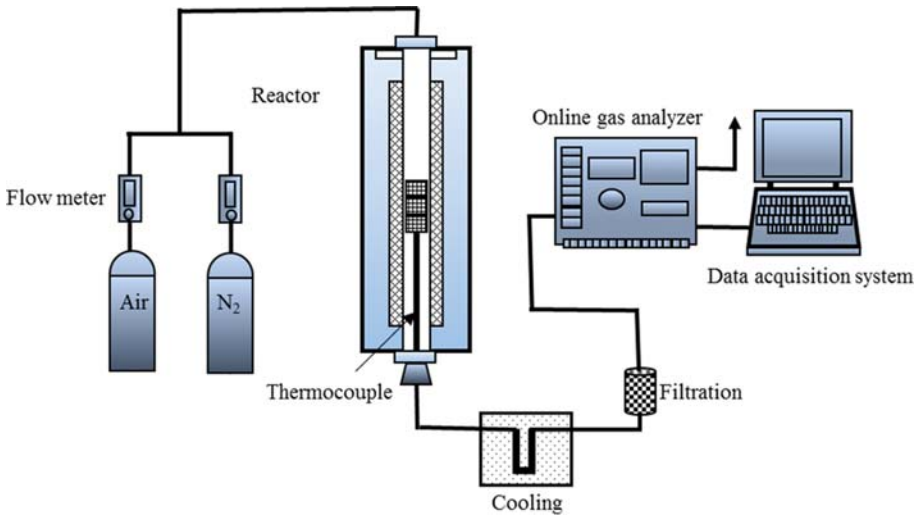

Fig. 1. Schematic view of the experimental fix-bed system of oxygen adsorption and desorption processes for oxygen carriers.

sample was heated to the desired temperature in N_2 to avoid oxygen absorption occurring. Then the gas was changed to absorption feed gas with certain oxygen concentration to investigate the oxygen absorption reactivity. After a thorough absorption process, the sample was heated to the desired desorption temperature, then the sample was exposed to N_2 to investigate the desorption reactivity. The online gas analyzer was placed at the outlet of reactor. The effect of air/N_2 in the hole system on the results was eliminated in the data process, described elsewhere in detail [37]. Before the fixed-bed tests, phase composition of the sample was performed by XRD (PANalytical, PW 3040/60; X'Pert Pro system with Cu Kα radiation). X-ray diffractogram of samples were recorded for 2θ between 10°-70° with a step scan of 0.02°. The microstructure of the sample was observed in a SUPERSCAN SSX-550 spectrometer system.

3. Sensitivity Evaluation Method

3-1. Data Analysis

In oxygen adsorption and desorption, the amount of oxygen intake (V_{oxi}), amount of oxygen release (V_{red}), and oxygen reaction (intake and release) rate (x) were obtained by the following equations [37,38].

For the oxygen adsorption process, data analysis is as follows:

$$V_{oxi}=\int_0^{t_{oxi}}(Q_{out'}\times C_{out'}-Q_{out}\times C_{out})dt \quad (1)$$

where, Q_{out} is the gas flow rate of the outlet gas, ml/min; C_{out} is the oxygen concentration of the outlet gas; $Q_{out'}$ is the gas flow rate of the outlet gas without reaction, ml/min; $C_{out'}$ is the oxygen concentration of the outlet gas without reaction, %; t_{oxi} is the oxygen intaking time, min.

On the basis of N_2 flow conservation for the inlet and outlet, we can get Eq. (2) and Eq. (3).

$$Q_{in}\times(100-C_{in})=Q_{out}\times(100-C_{out}) \quad (2)$$

$$Q_{in}\times(100-C_{in})=Q_{out'}\times(100-C_{out'}) \quad (3)$$

Combined with Eq. (1), Eq. (2) and Eq. (3), the following equation results:

$$V_{oxi}=\int_0^{t_{oxi}}(100-C_{in})\times Q_{in}\times\left(\frac{C_{out'}-C_{out}}{(1-C_{out})(1-C_{out'})}\right)dt \quad (4)$$

For the oxygen desorption process, data analysis is as follows:

$$V_{red}=\int_0^{t_{red}}100\times Q_{in}\times\left(\frac{C_{out'}-C_{out}}{(1-C_{out})(1-C_{out'})}\right)dt \quad (5)$$

where, t_{red} is the oxygen releasing time, min.

Oxygen releasing rate can be found by Eq. (6).

$$x=\frac{V_{oxi}}{t_{oxi}+t_{red}} \quad (6)$$

3-2. Multi-objective Comprehensive Evaluation Method

To deeply evaluate the intake/release behavior of oxygen carriers, a multi-objective comprehensive evaluation method was used to make the comprehensive indicator. In multi-objective comprehensive evaluation model, the condition is set as $A=A_1, A_2, \cdots A_n$, and indicator as $G=G_1, G_2, \cdots G_m$. Processes of establishing multi-objective comprehensive evaluation model are as the following [39].

(1) Non-dimension of indicators

$$z_{ij}=\frac{m_{ij}-m_j^{min}}{m_j^{max}-m_j^{min}} \quad (7)$$

where, i is condition, i=1, 2, ···· n; j is indicator, j=1, 2, ···· m; m_{ij} is value of indicator with condition i; m_j^{max} is the maximum value of indicator with condition i; m_j^{min} is the minimum value of indicator with condition i; z_{ij} is standard value of indicators with condition i.

(2) Comprehensive evaluation indicator

$$D_i(W)=\sum_{j=1}^{m}z_{ij}w_j \quad (8)$$

where, w_j is weight of G_j, $w_j=\delta(G_j)/\sum_{j=1}^{m}\delta(G_j)$, $\delta(G_j)$ is mean square variance of G_i.

3-3. Orthogonal Test Method

The orthogonal test results were analyzed with variance analysis [40]. In the analysis process, sum of squares (SS), mean squares

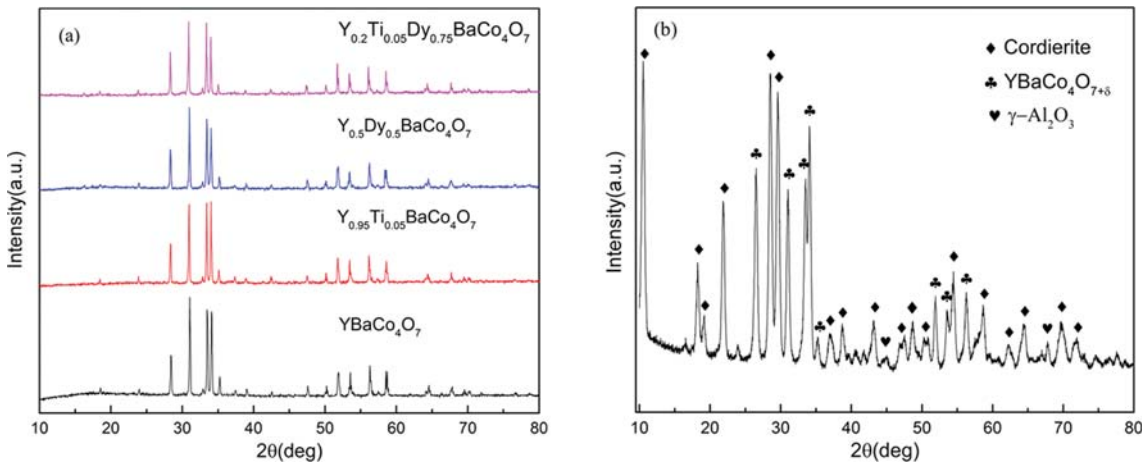

Fig. 2. Phase composition of (a) $YBaCo_4O_{7+\delta}$, $Y_{0.95}Ti_{0.05}BaCo_4O_{7+\delta}$, $Y_{0.5}Dy_{0.5}BaCo_4O_{7+\delta}$ and $Y_{0.2}Ti_{0.05}Dy_{0.75}BaCo_4O_{7+\delta}$ oxygen carriers and (b) $YBaCo_4O_{7+\delta}$ monolith sample.

(MS), degree of freedom (DF), max-min difference, error, sum of squares error (SS_e) and *F* value were calculated. In the orthogonal test, $Ln(r^m)$, the value of comprehensive evaluation indicator for orthogonal test is y_i (i=1, 2, 3, ···· n). The analysis process is as follows.

The total sum of squares (SS) can be found by Eq. (9).

$$SS_t=\sum_{i=1}^{n}(y_i-\overline{y}_i)^2 \tag{9}$$

The SS for every factor is from Eq. (10).

$$SS_j=\sum_{i=1}^{r}n_i(\overline{T}_i-\overline{y}_i)^2 \tag{10}$$

where, j is experimental factor (A-oxygen carrier, B-adsorption temperature, C-desorption temperature, D-gas flow, E-oxygen concentration). r is the level of every factor. n_i is test times under level i. $\overline{T}_i$ is average value of orthogonal test for factor A under level i. $\overline{y}_i$ is average value of orthogonal test.

The SS_e is by Eq. (11).

$$SS_e=SS_t-SS_j \tag{11}$$

The DF for every factor and DF for error are by Eq. (12).

$$DF_j=DF_e=r-1 \tag{12}$$

The MS for every factor and MS for error are by Eq. (13).

$$MS_j=\frac{SS_j}{DF_j},\ MS_e=\frac{SS_e}{DF_e} \tag{13}$$

The *F* value for every factor A (B, C, D, E) is from Eq. (14).

$$F_j=\frac{MS_j}{MS_e} \tag{14}$$

F value is used to evaluate the effect of the experimental factor on the comprehensive evaluation indicator. If $F_j>F_{0.01}(DF_j, DF_e)$, the effect of the experimental factor on the evaluation indicator is particularly significant, signed as '**'. If $F_{0.05}(DF_j, DF_e)$, $<F_j<F_{0.01}(DF_j, DF_e)$, the effect of the experimental factor on the evaluation indicator is more significant, signed as '*'. If $F_{0.10}(DF_j, DF_e)$, $<F_j<F_{0.05}(DF_j, DF_e)$, the effect of the experimental factor on the evaluation indicator is significant, signed as '(*)'. If $F_{0.25}(DF_j, DF_e)$, $<F_j<F_{0.10}(DF_j, DF_e)$, the experimental factor has no significant effect on the evaluation indicator but has some influence, signed as '[*]'. If $F_j<F_{0.25}(DF_j, DF_e)$, the effect of the experimental factor on the evaluation indicator is especially not significant, and there is no sign [41].

RESULTS AND DISCUSSION

1. Results and Analysis of XRD and SEM Characterization

Fig. 2(a) displays the phase composition of $YBaCo_4O_{7+\delta}$, $Y_{0.95}Ti_{0.05}BaCo_4O_{7+\delta}$, $Y_{0.5}Dy_{0.5}BaCo_4O_{7+\delta}$ and $Y_{0.2}Ti_{0.05}Dy_{0.75}BaCo_4O_{7+\delta}$ samples. With XRD data, the cell parameters of the samples were refined in the previous work [32]. The present samples are all single phase and indexed as $YBaCo_4O_{7+\delta}$ structure [31]. No minor phases were observed. There was no effect of partial substitution of Y with Ti or/and Dy on the phase composition of oxygen carriers. Fig. 2(b) displays the phase composition of $YBaCo_4O_{7+\delta}$ monolith sample. The $YBaCo_4O_{7+\delta}$ (space group $P6_3mc$), γ-Al_2O_3 (space group *Fd3m*), and cordierite (space group *P6/mcc*) are identified. They all keep the original phase, indicating that there is no reaction between the $YBaCo_4O_{7+\delta}$ oxygen carrier and Al_2O_3/cordierite in the process of calcination. It's really the same results for $Y_{0.95}Ti_{0.05}BaCo_4O_{7+\delta}$, $Y_{0.5}Dy_{0.5}BaCo_4O_{7+\delta}$ and $Y_{0.2}Ti_{0.05}Dy_{0.75}BaCo_4O_{7+\delta}$ oxygen carriers. Thus, the synthesis process and parameters of monolith sample were reasonable.

Fig. 3(a) and 3(c) display the micromorphology of cordierite at 40× magnification and 2000× magnification, respectively. Fig. 3(a) shows that the cordierite honeycomb was square and wall thickness was uniform. Fig. 3(c) shows that the micromorphology of cordierite honeycomb was speculate irregular polyhedron. Fig. 3(b) and 3(d) display the micromorphology of $Y_{0.5}Dy_{0.5}BaCo_4O_{7+\delta}$ monolith sample at 40× magnification and 2000× magnification, respectively. Fig. 3(b) shows that the cordierite honeycomb was covered uniformly by oxygen carrier. Fig. 3(d) shows that the micromorphology of oxygen carrier was spherical or sphere-like agglomerates.

2. Results and Analysis of Orthogonal Test

2-1. Results of Orthogonal Test

The oxygen adsorption and desorption behaviors of four oxygen

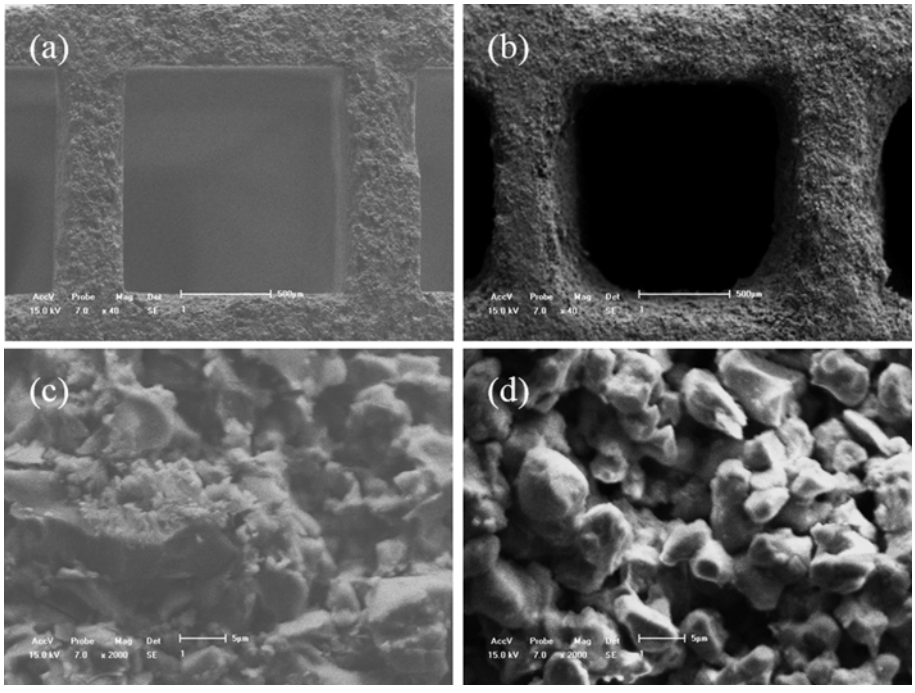

Fig. 3. SEM images at (a) 40× magnification and (c) 2000× magnification for cordierite honeycomb and SEM images at (b) 40× magnification and (d) 2000× magnification $Y_{0.5}Dy_{0.5}BaCo_4O_{7+\delta}$ monolith sample.

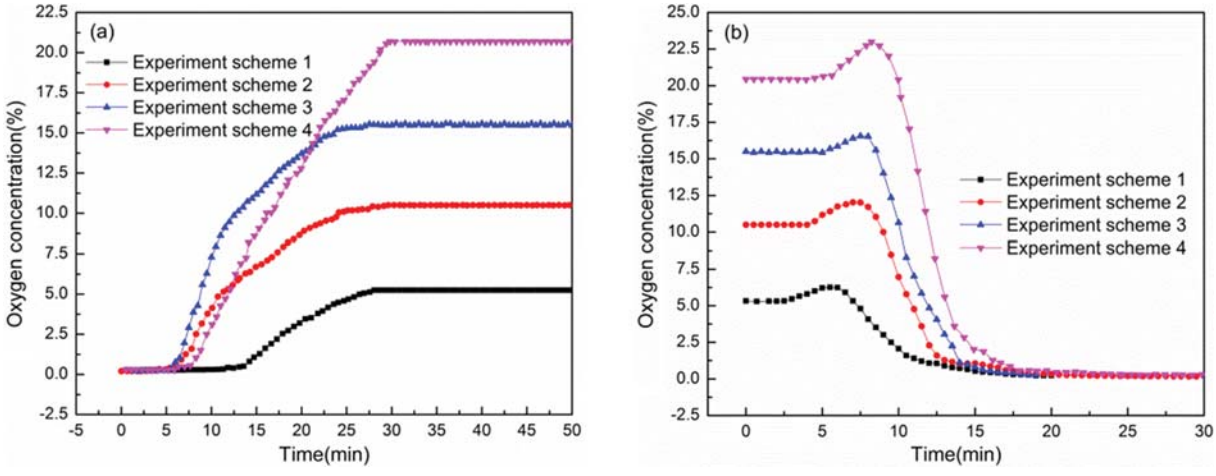

Fig. 4. The outlet oxygen concentration of $YBaCo_4O_{7+\delta}$ oxygen carrier at different experimental scheme measured during (a) the oxygen absorption process and (b) the oxygen desorption process.

carriers under different operating conditions were investigated in the fixed-bed reactor. Fig. 4 shows the outlet oxygen concentration under different operating conditions during oxygen absorption and desorption processes with $YBaCo_4O_{7+\delta}$ oxygen carrier. For oxygen absorption, the starting point time of the outlet oxygen concentration for different scheme is different, which may depend on the inlet gas flow rate, adsorption temperature, inlet oxygen concentration or the all of them. For oxygen desorption, the starting point and maximum point of the outlet oxygen concentration for different scheme is different, which depends on the desorption temperature, as only the desorption temperature is different for all the parameters of oxygen desorption process. The time of starting point and maximum point of the outlet oxygen concentration move forward to high values with increasing desorption temperature, which indicates that increasing desorption temperature is propitious to oxygen release.

The results show that the amount of oxygen intake can release under different desorption temperature; thus, the amount of maximum oxygen intake per unit mass ($V_{oxi''}$) was selected as evaluation indicator to express the oxygen storage capacity. Oxygen reaction rate per unit mass (x_r) was selected as evaluation indicator to express the reaction capacity. $V_{oxi''}$ and $x_{''}$ were selected as evaluation indicators. Table 2 shows the results of comprehensive evaluation indicators on the oxygen absorption and desorption processes of four

Table 2. Comprehensive evaluation indicator of oxygen carriers under different operating conditions

Experiment scheme	V_{oxi}/ml/g	x_v/ml/g·min	Comprehensive evaluation indicator
	0.4909	0.5091	
1	3.8713	0.0821	0.0690
2	6.0528	0.1357	0.2705
3	6.5095	0.1569	0.3352
4	13.9678	0.2906	0.9257
5	5.7376	0.1152	0.2125
6	2.5461	0.0759	0.0062
7	10.3913	0.1978	0.5706
8	9.8747	0.1700	0.4887
9	7.9130	0.2060	0.4981
10	15.9883	0.2634	0.9249
11	5.6208	0.1221	0.2238
12	5.4058	0.1364	0.2483
13	7.1617	0.1722	0.3940
14	7.9153	0.1591	0.3919
15	7.8610	0.1375	0.3411
16	2.7548	0.0732	0.0077

oxygen carriers. From Table 2, the values of evaluation indicators depend on the operating conditions. After eliminating the influence of dimension and obtaining the weight with mean square, the comprehensive evaluation indicator was obtained. The calculated value was used to evaluate the properties of oxygen absorption and desorption. The weights of V_{oxi} and x_v were 0.4909, and 0.5091, respectively.

2-2. Sensitivity Analysis of Experimental Factors

In the study, all the experimental factors were evaluated using an orthogonal $L_{16}(4^5)$ test design. According to the orthogonal test theory, the experimental tests are carried out by variance analysis. The results are shown in Table 3. T_1, T_2, T_3, and T_4 are the sum of comprehensive evaluation indicator for every experimental factor under the same level, respectively. $\overline{T}_1$, $\overline{T}_2$, $\overline{T}_3$, and $\overline{T}_4$ are average value of T_1, T_2, T_3, and T_4, respectively. $\overline{T}_1$, $\overline{T}_2$, $\overline{T}_3$, and $\overline{T}_4$ are used to evaluate the SS_j for every experimental factor. SS_t can be determined by the value and average value of the comprehensive evaluation indicator. SS_e can be obtained by SS_t and SS_j. Thus, MS and *F*-value can be found, which is shown in Table 4. According to *F*-value, the effect degree of experimental factors can be obtained.

For the given experimental factors, values of experimental factors, and the evaluation indicator, the analysis of variance shows

Table 3. Experiment scheme and data analysis

Experiment scheme	Oxygen carrier	Absorption temperature/°C	Desorption temperature/°C	Gas flow/ ml/min	Oxygen concentration/%	Comprehensive evaluation indicator
1	1	1	1	1	1	0.0690
2	1	2	4	3	2	0.2705
3	1	3	2	4	3	0.3352
4	1	4	3	2	4	0.9257
5	2	1	2	2	2	0.2125
6	2	2	3	4	1	0.0062
7	2	3	1	3	4	0.5706
8	2	4	4	1	3	0.4887
9	3	1	3	3	3	0.4981
10	3	2	2	1	4	0.9249
11	3	3	4	2	1	0.2238
12	3	4	1	4	2	0.2483
13	4	1	4	4	4	0.3940
14	4	2	1	2	3	0.3919
15	4	3	3	1	2	0.3411
16	4	4	2	3	1	0.0077
T_1	1.6005	1.1736	1.2798	1.8238	0.3067	
T_2	1.2780	1.5935	1.4803	1.7539	1.0724	
T_3	1.8952	1.4708	1.7712	1.3469	1.7140	
T_4	1.1348	1.6704	1.3771	0.9838	2.8153	
$\overline{T}_1$	0.4001	0.2934	0.3199	0.4559	0.0767	
$\overline{T}_2$	0.3195	0.3984	0.3701	0.4385	0.2681	
$\overline{T}_3$	0.4738	0.3677	0.4428	0.3367	0.4285	
$\overline{T}_4$	0.2837	0.4176	0.3443	0.2459	0.7038	
R	0.1901	0.1242	0.1229	0.2100	0.6271	
SS_j	0.0867	0.0358	0.0339	0.1143	0.8437	
SS_t			1.1157			
SS_e			0.0286			

Table 4. Analysis of variance

Source	SS	DF	MS	*F*-value	Degree of significance
A	0.0867	3.0000	0.0289	3.0344	[*]
B	0.0358	3.0000	0.0119	1.2517	
C	0.0339	3.0000	0.0113	1.1850	
D	0.1143	3.0000	0.0381	4.0000	[*]
E	0.8437	3.0000	0.2812	29.5267	**
Error	0.0286	3.0000	0.0095		

that oxygen concentration is the most important factor in oxygen absorption. Ion-substitution and gas flow rate have no significant effect (have some influence) on the oxygen absorption/desorption properties. The effect of absorption and desorption temperature on the oxygen absorption/desorption properties is especially not significant. It can be seen from Table 4 that the influence level of operating conditions on oxygen absorption/desorption properties varies in the order: E>D=A>B=C.

2-3. Optimum Analysis of Experimental Factors

The orthogonal test, a scientific and systematic method [42], was used to optimize the operating conditions for the oxygen absorption/desorption properties. This test has advantages such as reducing the testing treatments and analyzing results scientifically [40]. Max-min difference, obtained by equation of $\max(\overline{T}_i)$-$\min(\overline{T}_i)$, signed as R, is displayed in Table 3. R=0.6271 is the maximum one, indicating that the most significant factor is oxygen concentration. The plots of y_i vs ($\overline{T}_i$) can be used to optimize the operating conditions, see Fig. 5. For experimental factor A, varying has no practical meaning, as experimental factor A is oxygen carrier. The "vary" certifies that $Y_{0.5}Dy_{0.5}BaCo_4O_{7+\delta}$ oxygen carrier shows best oxygen absorption and desorption properties. The optimum operating conditions such as absorption temperature, 350 °C, desorption temperature, 430 °C, gas flow rate, 200 ml/min, and oxygen concentration, 21% were confirmed.

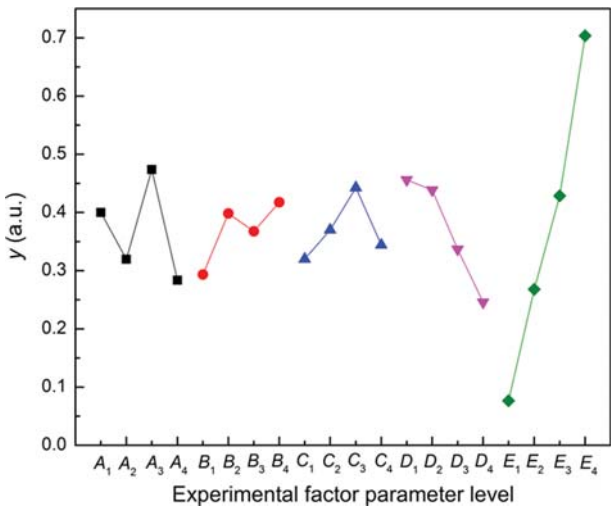

Fig. 5. Effects of parameter level of experimental factor A, B, C, and D on comprehensive evaluation indicator.

CONCLUSIONS

Oxygen carriers with monolithic configurations were developed. The sensitivity of operation parameters and optimal operation parameters were investigated with monolithic oxygen carriers by orthogonal experiment. The amount of maximum oxygen intaking per unit mass and oxygen reaction rate per unit mass were selected as evaluation indicators. The comprehensive evaluation indicator was obtained by the analysis of mean square variance. The results of variance analysis showed that the influence level of operating conditions on oxygen absorption/desorption properties varied in the order: oxygen concentration>gas flow rate>absorption temperature= desorption temperature. Analysis of max-min difference showed that the optimum operating conditions such as absorption temperature, 350 °C, desorption temperature, 430 °C, gas flow rate, 200 ml/min, and oxygen concentration, 21% were confirmed.

ACKNOWLEDGEMENTS

This study was financially supported by National Natural Science Foundation of China (Grant No. 51576035, 51604078), Fundamental Research Funds for the Central Universities (Grant No. N162504012), and Post-Doctoral Science Foundation (Grant No. 2017M610185, 20170101).

NOTES

The authors declare no competing financial interest.

REFERENCES

1. Q. Yang and J. Y. S. Lin, *Sep. Purif. Technol.*, **49**(1), 27 (2006).
2. B. Moghtaderi, *Energy Fuels*, **24**(1), 190 (2010).
3. H. Song, K. Shah, E. Doroodchi and B. Moghtaderi, *Energy Fuels*, **28**(1), 163 (2014).
4. H. Song, K. Shah, E. Doroodchi, T. Wall and B. Moghtaderi, *Energy Fuels*, **28**(1), 173 (2014).
5. S. Y. Chuang, J. S. Dennis, A. D. Hayhurst and S. A. Scott, *Combust. Flame*, **154**(1-2), 109 (2008).
6. K. Wang, Q. B. Yu and Q. Qin, *Energy Fuels*, **27**(9), 5466 (2013).
7. K. Wang, Q. B. Yu, Q. Qin, J. Z. Li and Z. M. Wang, *J. Inorg. Mater.*, **29**(3), 301 (2014).
8. M. Ishida, M. Yamamoto and T. Ohba, *Energy Convers. Manag.*, **43**(9-12), 1469 (2002).
9. T. Mattisson, A. Lyngfelt and H. Leion, *Int. J. Greenhouse Gas Control.*, **3**(1), 11 (2009).
10. M. Arjmand, A. Azad, H. Leion, A. Lyngfelt and T. Mattisson, *Energy Fuels*, **25**(11), 5493 (2011).
11. A. Shulman, E. Cleverstam, T. Mattisson and A. Lyngfelt, *Fuel*, **90**(3), 941 (2011).
12. G. Azimi, H. Leion, T. Mattisson and A. Lyngfelt, *Energy Procedia*, **4**(1), 370 (2011).
13. K. Zhao, F. He, Z. Huang, G. Q. Wei, A. Q. Zheng, H. B. Li and Z. L. Zhao, *Korean J. Chem. Eng.*, **34**(6), 1651 (2017).
14. B. Y. Kwak, N. K. Park, J. I. Baek, H. J. Ryu and M. Kang, *Korean J. Chem. Eng.*, **34**(7), 1936 (2017).

15. Z. Cheng, L. Qin, J. A. Fan and L.-S. Fan, *Eng.*, DOI:https://doi.org/10.1016/j.eng.2018.05.002.
16. M. M. Hossain, *Arab. J. Sci. Eng.*, 1 (2017), DOI:10.1007/s13369-017-2706-9.
17. J. Zhu, W. Wang, S. J. Lian, X. N. Hua and Z. Xia, *J. Mater. Cycles Waste*, **19**(1), 453 (2017).
18. W. Q. Shen, MA Diss., Huazhong University of Science and Technology (2012).
19. T. Zhang, Z. S. Li and N. S. Cai, *J. Chem. Eng.*, **26**(3), 845 (2009).
20. M. Valldor and M. Andersson, *Solid State Sci.*, **4**(7), 923 (2002).
21. M. Karppinen, H. Yanauchi and S. Otani, *Chem. Mater.*, **18**(2), 490 (2006).
22. T. Motohashi, S. Kadita, H. Fjellvag, M. Karppinen and H. Yamauchi, *Mater. Sci Eng. B.*, **148**(1), 196 (2008).
23. Y. Nagai, T. Yamamoto, T. Tanaka, S. Yoshida, T. Nonaka, T. Okamoto, A. Suda and M. Sugiura, *Catal. Today*, **74**(3-4), 225 (2007).
24. J. Kašpar and P. Fornasiero, *J. Solid State Chem.*, **171**(1-2), 19 (2003).
25. S. Kadota, M. Kappinen, T. Motohashi and H. Yamauchi, *Chem. Mater.*, **20**(20), 6378 (2008).
26. S. Wang, H. S. Hao, B. F. Zhu, J. F. Jia and X. Hu, *J. Mater. Sci.*, **43**(15), 5385 (2008).
27. S. M. Zhang, MA Dissertation, ZhengZhou University (2011).
28. L. J. Guo, MA Dissertation, ZhengZhou University (2005).
29. L. P. Kozeeva, M. Y. Kameneva, A. N. Lavrov and N. V. Podberezskaya, *Inorg. Mater.*, **49**(6), 626 (2013).
30. O. Parkkima, H. Yamauchi and M. Karppinen, *Chem. Mater.*, **25**(4), 599 (2013).
31. M. Valldor, *Solid State Sci.*, **7**(10), 1163 (2005).
32. L. M. Hou, Q. B. Yu, T. Wang, K. Wang, Q. Qin and Z. F. Qi, *Korean J. Chem. Eng.*, **35**(3), 626 (2018).
33. A. D. Qi, S. D. Wang, G. Z. Fu, C. J. Ni and D. Y. Wu, *Appl. Catal. A: Gen.*, **281**(1-2), 233 (2005).
34. B. B. Shi and Z. D. Jiang, *Nat. Gas Chem. Ind.*, **38**(3), 11 (2013).
35. K. Wang, MA Diss., Shanghai Jiaotong University (2009).
36. S. Cimino, L. Lisi, R. Pirone, G. Russo and M. Turco, *Catal. Today*, **59**(1), 19 (2000).
37. K. Wang, Q. B. Yu, Q. Qin, Z. L. Zuo and T. W. Wu, *Chem. Eng. J.*, **287**, 292 (2016).
38. Q. Liu, J. J. Shi, S. D. Zheng, M. N. Tao, Y. He and Y. Shi, *Ind. Eng. Chem. Res.*, **53**(29), 11677 (2014).
39. M. T. Wang, *Chin. Soft Sci.*, **08**, 100 (1999).
40. H. L. Ni, Z. Y. Wu, I. Muhammad, Z. Y. Lu and J. C. Li, *Bra J. Pharmacogn.*, **28**(2), 151 (2018).
41. Y. J. Zuo, MA Diss., Guangdong University Technology (2012).
42. F. Kong, Y. Bi, C. Yan and Z. Zeng, *J. Med. Plants Res.*, **7**(12), 720 (2013).